Available online at www.sciencedirect.com
SCIENCE DIRECT®
PERGAMON
Polyhedron 22 (2003) 2447–2452
POLYHEDRON
www.elsevier.com/locate/poly

Magnetic and electrical properties of (DT-TTF)$_4$[Au(pds)$_2$]$_3$

João C. Dias [a,1], Jorge Morgado [b,2], Helena Alves [a,1], Elsa B. Lopes [a,1], Isabel C. Santos [a,1], M.T. Duarte [a,1], R.T. Henriques [b,2], Manuel Almeida [a,1,*], Xavier Ribas [c,3], Concepció Rovira [c,3], Jaume Veciana [c,3]

[a] *Departamento de Química, Instituto Tecnológico e Nuclear, P 2686-953 Sacavem, Portugal*
[b] *Departamento de Engenharia Química, Instituto Superior Técnico, Lisbon, Portugal*
[c] *Instituto de Ciència de Materiales de Barcelona, CSIC, Campus de la UAB, E-08193 Belaterra, Spain*

Received 29 October 2002; accepted 8 January 2003

Abstract

The charge transfer salt (DT-TTF)$_4$[Au(pds)$_2$]$_3$ (DT-TTF, $\Delta^{2,2'}$-bithieno[3,4-d]-1,3-dithiol; pds, pyrazine-2,3-diselenate) was prepared and characterised by X-ray diffraction, electrical conductivity, thermoelectric power, magnetic susceptibility and EPR measurements. This compound crystallises in the triclinic system, space group $P\bar{1}$, with the unit cell parameters $a = 9.712(5)$ Å, $b = 13.620(5)$ Å, $c = 17.169(5)$ Å, $\alpha = 97.254(5)^\circ$, $\beta = 106.132(5)^\circ$, $\gamma = 95.956(5)^\circ$, $V = 2141.10(15)$ Å^3, $Z = 1$. Its crystal structure consists of a bidimensional network of DT-TTF tetramers and orthogonal anions. The electrical properties indicate it is a small gap semiconductor ($2\Delta = 190$ meV), with a room temperature conductivity of $\sigma_{RT} = 2$ S cm^{-1}. The electrical and magnetic properties reveal two types of transitions occurring upon cooling. The first, at 238 K, as a second order change to a large gap semiconducting state and, a lower transition, of first order type, with a large hysteresis between 210 and 150 K, probably associated with a larger structural change in the DT-TTF network.

Keywords: Dithiolates; Gold(III) complexes; Crystallographic studies; Magnetic properties; Electrical transport properties; Charge-transfer salts

1. Introduction

The discovery of a spin-ladder behaviour in the (DT-TTF)$_2$[Au(mnt)$_2$] compound, the first example of such a molecule based organic system [1,2], lead us to explore new compounds based on this donor and similar transition metal complexes, aiming at finding other systems in which a spin-ladder behaviour could be also observed and obtain more detailed structure/properties relationship. With such a purpose in mind we selected the [Au(pds)$_2$] (pds, pyrazine-2,3-diselenate) complex which, as a gold(III) diamagnetic species of comparable shape and dimensions as [Au(mnt)$_2$], was thought could lead to a compound with a behaviour similar to that of (DT-TTF)$_2$[Au(mnt)$_2$] (Scheme 1).

The compound obtained by the combination of the DT-TTF donor with [Au(pds)$_2$] has however a quite different stoichiometry: (DT-TTF)$_4$[Au(pds)$_2$]$_3$. In this paper, we describe the synthesis and characterisation of this compound which, upon cooling, undergoes an unusual sequence of two phase transitions at 238 and ~ 150 K.

2. Experimental

2.1. Synthesis

The pyrazine-2,3-diselenate ligand, pds^{2-}, was synthesized as the sodium salt, Na$_2$(pds), following a previously reported procedure for the preparation of the sulfur analogue [3]. The gold complex was prepared in water, by reaction of Na$_2$(pds) with KAuCl$_4$, and

* Corresponding author. Tel.: +351-21-994-6171; fax: +351-21-994-1455.
E-mail address: malmeida@itn.pt (M. Almeida).
[1] malmeida@itn.pt.
[2] rth@ist.utl.pt.
[3] cun@icmab.es.

0277-5387/03/$ - see front matter
doi:10.1016/S0277-5387(03)00210-9

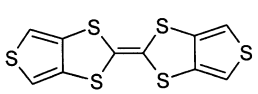

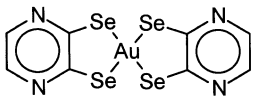

Scheme 1.

precipitated as the tetrabutylammonium salt, (NBu$^{n}_{4}$)[Au(pds)$_2$], by addition of tetrabutylammonium chloride. The product was recrystallised from acetone–hexane. The DT-TTF, $\Delta^{2,2'}$-bithieno[3,4-d]-1,3-dithiol, was synthesised as previously described in the literature [4].

(DT-TTF)$_4$[Au(pds)$_2$]$_3$ as needle shaped dark crystals was obtained by electrocrystallisation from solutions of DT-TTF and (NBu$^{n}_{4}$)Au(pds)$_2$ in dichloromethane, under galvanostatic conditions and using platinum electrodes (current density ≈ 2 μA cm^{-2}). Needle shaped dark crystals with metallic shine, typically $5 \times 0.1 \times 0.05$ mm^3 were collected from the anode after ~ 7 days by filtering and washed with cold dichloromethane. (Found: C, 22.15%; H, 0.91%; N, 5.08%; S, 23.28%. $C_{64}H_{28}N_{12}S_{24}Se_{12}Au_3$ requires C, 23.49%; H, 0.86%; N, 5.14%; S, 23.51%.)

2.2. X-Ray structure determination

A needle shaped dark crystal of (DT-TTF)$_4$[Au(pds)$_2$]$_3$, with approximate dimensions $1.0 \times 0.4 \times 0.08$ mm^3, was used for data collection on a Enraf–Nonius TURBO CAD4 diffractometer equipped with a graphite monochromatised Cu Kα radiation ($\lambda =$ 1.5418 Å) in the $\omega-2\theta$ scan mode at room temperature. The data were corrected for Lorentz and polarisation effects and empirical absorption corrections based on Ψ-scans were applied. The structure was solved by direct methods using SIR-97 [5] and refined by full-matrix least-squares methods using the program SHELXL-97 [6] and the WINGX software package [7]. All non-hydrogen atoms were refined anisotropically. Hydrogen atoms were placed in calculated positions. Molecular graphics were prepared with SCHAKAL-97 [8]. Crystal data and structure refinement are summarized in Table 1.

2.3. Electrical transport measurements

The electrical resistivity and the thermoelectric power were measured along the longer axis of the same crystal, placed in a cell attached to the cold stage of a closed-cycle helium refrigerator with accessible temperature in the range 16–310 K. In a first step, the thermoelectric power was measured using a slow AC technique [9] in an apparatus similar to that described by Chaikin and Kwak [10]. The thermal gradients were kept below 1 K and monitored by a Au(0.07 at.% Fe)-chromel thermocouple measured with a Keithley 181 nanovoltmeter. A similar thermocouple was used to measure the temperature of the sample. The extremities of the sample were directly glued with platinum paint (Demetron 308A) to the $\phi = 25$ μm gold wires (Goodfellow, 99.99% pure) thermally anchored to two quartz blocks. The thermoelectric voltage was measured by a Keithley 181 nanovoltmeter and the absolute thermopower was calculated after the correction for the absolute thermopower of gold using the data of Huebner [11]. In a second step the electrical resistance was measured with the four-in line contacts technique by placing two extra contacts on the sample without removal from its holder. At higher temperatures a current of 1 μA was passed through the sample at low frequency (77 Hz) and the voltage drop measured with a lock-in amplifier. At the lower temperature range, where the sample impedance was higher than 10 MΩ measurements were performed with a d.c. technique, the voltage drop was measured with an electrometer (Keithley 619) with both direct and reverse current of ~ 1 μA.

Table 1
Crystal data and structure refinement of (DT-TTF)$_4$[Au(pds)$_2$]$_3$

Empirical formula	$C_{64}H_{28}Au_3N_{12}S_{24}Se_{12}$
Formula weight	3272.84
Crystal system	Triclinic
Space group	$P\bar{1}$
Unit cell dimensions	
a (Å)	9.7118(9)
b (Å)	13.6202(10)
c (Å)	17.1685(15)
α (°)	97.254(6)
β (°)	106.132(7)
γ (°)	95.956(7)
V (Å^3)	2141.1(15)
Z	1
D_{calc} (Mg m^{-3})	2.538
μ (mm^{-1})	21.196
$F(0\,0\,0)$	1525
2θ, Range (°)	3.31–67.01
h, k, l, Ranges	0/11, −16/16, −20/19
Reflections collected/unique	8103/7613 [$R_{int} = 0.0523$]
Data/parameters	7613/521
Completeness to theta	99.5%
Absorption correction	Psi-scan
Transm—max/min	0.9873/0.6013
Goodness-of-fit on F^2	0.967
R [$I > 2\sigma(I)$]	0.0697
wR	0.1591

2.4. Magnetic measurements

Static magnetic susceptibility measurements were performed in the temperature range 2–300 K using a Faraday system (Oxford Instruments) equipped with a 7 T superconducting magnet. The magnetisation measurements were performed under a static magnetic field of 5 T. The force on the polycrystalline samples, contained in a previously measured thin-walled Teflon bucket, was

measured with a microbalance (Sartorius S3D-V) applying forward and reverse gradients of 1 T m^{-1}. The paramagnetic susceptibility was calculated considering a diamagnetic correction estimated from tabulated Pascal constants.

EPR spectra were obtained in a conventional X-band spectrometer (Bruker ESP 300 E) equipped with a microwave bridge ER041XK, a rectangular cavity operating in T102 mode, a field controller ER 032M system and a Oxford ESR-900 cryostat, which enabled measurements in the temperature range 4–300 K and the temperature was monitored by a Au(0.07 at.% Fe)-chromel thermocouple placed close to the sample. The measurements were performed on single crystals, placed inside a quartz tube. The modulation amplitude was kept well below the line width and the microwave power well below saturation.

3. Results and discussion

3.1. Structural characterisation

$(DT\text{-}TTF)_4[Au(pds)_2]_3$ crystallises in the triclinic system, space group $P\bar{1}$, with the unit cell parameters given in Table 1. The asymmetric unit contains two independent donor units in general position ((DT-TTF(1) and DT-TTF(2)), one $[Au(pds)_2](1)$ complex at a general position and one half of a second $[Au(pds)_2](2)$ complex with the metal on an inversion centre.

The two DT-TTF units present identical bond lengths within experimental error. The DT-TTF(1) unit presents a small boat distortion with a deviation of the outer sulfur atoms, S3 and S6, from the average plane of 0.2025 and 0.1843 Å, respectively, while the DT-TTF(2) unit is almost planar. The $[Au(pds)_2](2)$ complex presents a small chair distortion, the pyrazine rings making an angle of 7.65° in relation to the central plane defined by the metal and the four selenium atoms. Table 2 presents the selected bonds and angles for the two independent $Au(pds)_2$ and (DT-TTF) units.

Four DT-TTF units related by an inversion centre ((DT-TTF(1), DT-TTF(2), (DT-TTF(2*) and DT-TTF(1*)), are stacked with a similar slipping along the short axis of these units, with average interplanar distances of 3.9332 and 3.5243 Å for (1)–(2) and (2)–(2*), respectively, and there are several S···S contacts between these units, which are below the sum of the van der Waals radii. These donor tetrads, stacked approximately along $a+b$, are flanked by the almost orthogonal $[Au(pds)_2]^-(1)$ (76°) and $[Au(pds)_2]^-(2)$ (88°) complexes. However, the end units of the tetrads (DT-TTF(1)) are connected to two other tetrads, by other S···S contacts only slightly above the sum of van der Waals radii and therefore there is a bidimensional network of short interdonor S···S contacts in the a, b plane (see Table 3). Along c these donor layers alternate with layers of $[Au(pds)_2](2)$ which lie almost paralell to the a, b plane. The almost planar $[Au(pds)_2](1)$ complex lies parallel to the b, c plane and nearly perpendicular (87.37°) to the $[Au(pds)_2](2)$ units (Figs. 1 and 2).

There are also several short contacts (smaller then the sum of the van der Waals radii) between sulfur atoms of the DT-TTF units and gold and selenium atoms of the $[Au(pds)_2]$ complexes, which are listed in Table 3. Especially significant are Au1–S2 at 3.571(6) Å, Au1–S7 at 3.401(6) Å and Au2–S3 at 3.810(5) Å.

Table 2
Selected bond lengths (Å) and angles (°) for $(DT\text{-}TTF)_4[Au(pds)_2]_3$

Au(1)–Se(1)	2.4157(19)	Au(1)–Se(2)	2.4213(19)
Au(1)–Se(4)	2.425(2)	Au(1)–Se(3)	2.4353(19)
Au(2)–Se(6)	2.426(3)	Au(2)–Se(6)#1	2.426(3)
Au(2)–Se(5)	2.431(2)	Au(2)–Se(5)#1	2.431(2)
Se(1)–C(1)	1.866(17)	Se(3)–C(6)	1.877(16)
Se(2)–C(2)	1.902(17)	Se(4)–C(5)	1.908(16)
Se(5)–C(10)	1.88(2)	Se(6)–C(9)	1.924(18)
Se(1)–Au(1)–Se(2)	91.12(7)	Se(1)–Au(1)–Se(4)	87.53(7)
Se(2)–Au(1)–Se(4)	177.76(8)	Se(1)–Au(1)–Se(3)	178.47(7)
Se(2)–Au(1)–Se(3)	89.71(7)	Se(4)–Au(1)–Se(3)	91.68(7)
Se(6)–Au(2)–Se(5)#1	88.55(8)	Se(6)–Au(2)–Se(5)	91.45(8)
S(1)–C(14)	1.749(18)	S(1)–C(16)	1.741(16)
S(2)–C(14)	1.725(18)	S(2)–C(15)	1.744(17)
S(3)–C(17)	1.680(19)	S(3)–C(18)	1.716(19)
S(4)–C(19)	1.736(15)	S(4)–C(13)	1.744(17)
S(5)–C(20)	1.707(17)	S(5)–C(13)	1.742(17)
S(6)–C(22)	1.694(19)	S(6)–C(21)	1.74(2)
S(7)–C(25)	1.716(17)	S(7)–C(24)	1.752(19)
S(8)–C(26)	1.745(16)	S(8)–C(24)	1.752(18)
S(9)–C(28)	1.690(19)	S(9)–C(27)	1.705(19)
S(10)–C(23)	1.712(17)	S(10)–C(29)	1.749(18)
S(11)–C(30)	1.711(16)	S(11)–C(23)	1.758(19)
S(12)–C(31)	1.68(2)	S(12)–C(32)	1.68(2)

Symmetry operations used to generate equivalent atoms: #1: $-x$, $-y$, $-z$.

Table 3
Short contact distances (Å) for $(DT\text{-}TTF)_4[Au(pds)_2]_3$

Atoms	Distance	Atoms	Distance
Between $[Au(pds)_2]$ and DT-TTF units			
Au1–S2[a]	3.571(6)	Au2–S3[c]	3.810(5)
Au1–S7[b]	3.401(6)	Au2–S3[d]	3.810(5)
Se1–S4[b]	3.537(5)	Se1–S1[b]	3.675(5)
Se2–S11[a]	3.535(6)	Se2–S8[a]	3.678(6)
Se3–S8[a]	3.554(6)	Se4–S1[b]	3.589(5)
Se4–S4[c]	3.691(5)	Se5–S3[d]	3.589(5)
Between DT-TTF units			
Intratetrads		Intertetrads	
S1–S7[a]	3.465(7)	S1–S1	4.001(7)[f]
S2–S8[a]	3.597(8)	S1–S4	3.826(7)[f]
S4–S10[a]	3.457(7)	S2–S2	4.133(8)[b]
S5–S11[a]	3.595(8)	S2–S5	4.119(8)[b]
S7–S10[e]	3.682(8)		

Symmetry operations: [a] x, y, z; [b] $-1+x$, y, z; [c] $1-x$, $-y$, $1-z$; [d] $-1+x$, y, $-1+z$; [e] $2-x$, $1-y$, $1-z$; [f] $2-x$, $-y$, $1-z$.

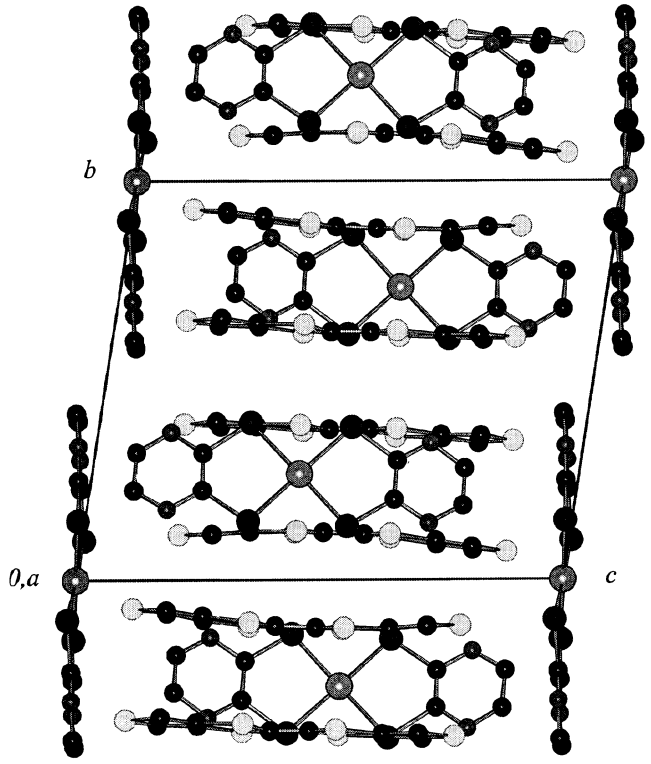

Fig. 1. View of the crystal structure of $(DT\text{-}TTF)_4[Au(pds)_2]_3$ along a.

3.2. Electrical transport properties

Electrical conductivity, σ, at room temperature was found to be $\sigma_{RT} = 2$ S cm^{-1}, following a thermally activated behaviour with an activation energy of $E_a = 95$ meV (see Fig. 3). However this activation energy is not temperature independent. Upon cooling, a faster increase of the electrical resistivity is observed below 235 K and the apparent activation energy, $-\mathrm{d}\ln\sigma/\mathrm{d}(1/T)$, shows a very sharp maximum at 238 K (inset in Fig. 3). This maximum is indicative of a second order phase transition associated with an increase of the electronic energy gap or a decrease of mobility.

Upon further cooling, at ~ 150 K electrical conductivity measurements show a subsequent transition towards a higher conductivity semiconducting phase, with approximately the same activation energy. This transition is characterised by a large hysteresis in the range 120–200 K. The magnitude of this hysteresis and the details of the $\sigma(T)$ curves are dependent on the thermal rates used during cycling. This behaviour is indicative of a sluggish first order structural transition.

Thermoelectric power measurements (Fig. 4) confirm the two transitions seen by electrical conductivity. At room temperature thermopower is negative and presents down to 238 K, an almost temperature independent value of approximately -60 μV K^{-1}. Below this temperature it starts to gradually decrease. At lower temperatures, in the range 130–215 K, the thermopower results show also an hysteresis similar to that previously described for conductivity, with negative or positive values on heating or cooling, respectively, and with a behaviour that, again, slightly depends on the heating and cooling rates during thermal cycling.

The temperature independent thermopower value of -60 μV K^{-1}, in the higher temperature range (above the second order phase transition at 238 K), is close to the spin only entropy value $S = (k_B/e)\ln 2$, predicted by a model of strongly localised carriers [12], and, therefore, is consistent with the semiconducting behaviour of the electrical conductivity.

3.3. Magnetic properties

The paramagnetic molar susceptibility, χ_p, as obtained from the magnetisation measurements, considering a diamagnetic contribution, estimated from Pascal constants as $\chi_d = -9.82 \times 10^{-4}$ emu mol^{-1}, is plotted as a function of the temperature in Fig. 5. At room temperature $\chi_p = 10.87 \times 10^{-4}$ emu mol^{-1} and increases upon cooling, following approximately a Curie–Weiss law, with an effective magnetic moment of $1.6\mu_B$, until approximately 180 K. The phase transition seen by electrical transport measurements at 238 K is barely seen in magnetization as only a very small perturbation is observed. However, the first order phase

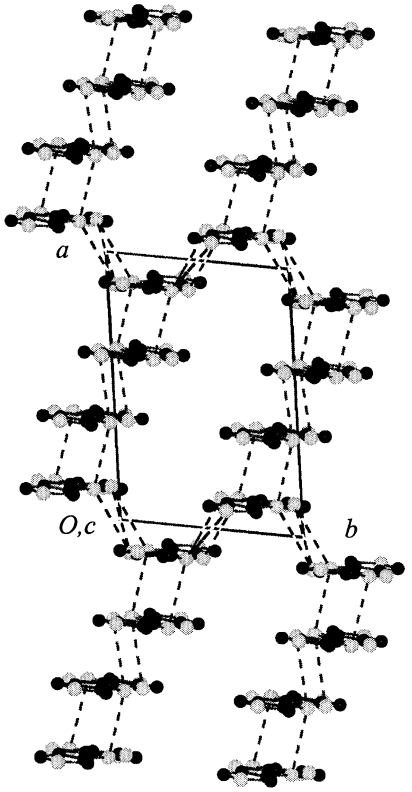

Fig. 2. Network of donor–donor contacts in $(DT\text{-}TTF)_4[Au(pds)_2]_3$ viewed along c. For clarity the $Au(pds)_2$ complexes were omitted.

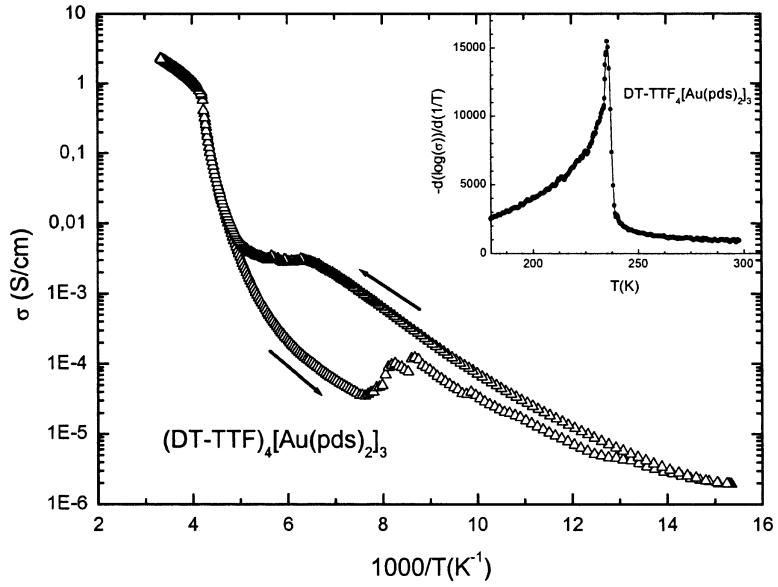

Fig. 3. Electrical conductivity, σ of a (DT-TTF)$_4$[Au(pds)$_2$]$_3$ single crystal as a function of the inverse absolute temperature, T. The inset shows the derivative—d ln σ/d(1/T) near the upper transition temperature.

transition is clearly observed, as a significant decrease of the effective magnetic moment of about 9% with, again, a large hysteresis behaviour between 90 and 180 K.

EPR measurements at room temperature on a single crystal show a single line 1.910 mT-wide centred at g-values in the range 2.0046 (horizontal crystal) to 2.0097 (vertical crystal, needle axis perpendicular to the horizontal magnetic field), dependent on the crystal orientation. These g-values are typical of oxidized DT-TTF, consistent with only one orientation of these donor units in the crystal structure and, as expected for this compound, with a diamagnetic $[Au(pds)_2]^-$ complex. At about 238 K it is observed a minimum, both in the linewidth (1.5 mT) and in the g-value, corresponding to the second order phase transition already discussed. Associated with the low temperature transition it is observed the appearance of a second narrower line, centred with the previous one. A clear hysteresis in g-values is also observed in the temperature range of the low temperature transition, between values of $g = 2.0098$ at high temperatures and $g = 2.0105$ at low temperatures. This hysteresis in g-values indicates that the low temperature transitions involves some reorientation of the DT-TTF molecules.

3.4. Final conclusion

The 4:3 stoichiometry observed for (DT-TTF)$_4$[Au(pds)$_2$]$_3$ is quite unusual for charge transfer salts in general and it is indeed the first time it is observed in salts with thiophene fused TTF type donors.

The average oxidation state of the donor in this compound as (DT-TTF)$_4^{3+}$ and their extended bidimensional network of interactions could lead to a partially (5/8) filled band. However, metallic properties in this (5/8) filled band are expected to occur only with an almost regular network with relatively large interactions. In this case, the strong tetramerisation of the donor units and the modulation of interdonor interactions in the a, b plane are seen as responsible for the semiconducting properties and the charge localisation, observed both in transport and magnetic properties.

The high temperature first order transition is probably driven by the electronic energy and possibly associated with any minor change in the structure and packing motif of the DT-TTF tetramers, which can easily change to a more or less anisotropic network of interactions. The lower transition, with its large and sluggish hysteresis is certainly a larger structural modification involving some DT-TTF reorientation. However, further structural work, namely by X-ray

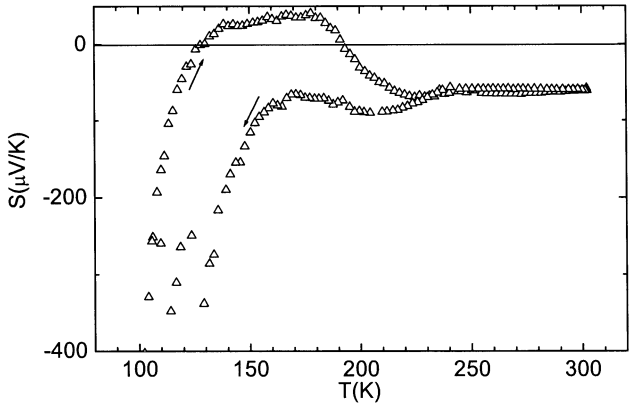

Fig. 4. Absolute thermopower of a (DT-TTF)$_4$[Au(pds)$_2$]$_3$ single crystal, S, as a function of temperature, T.

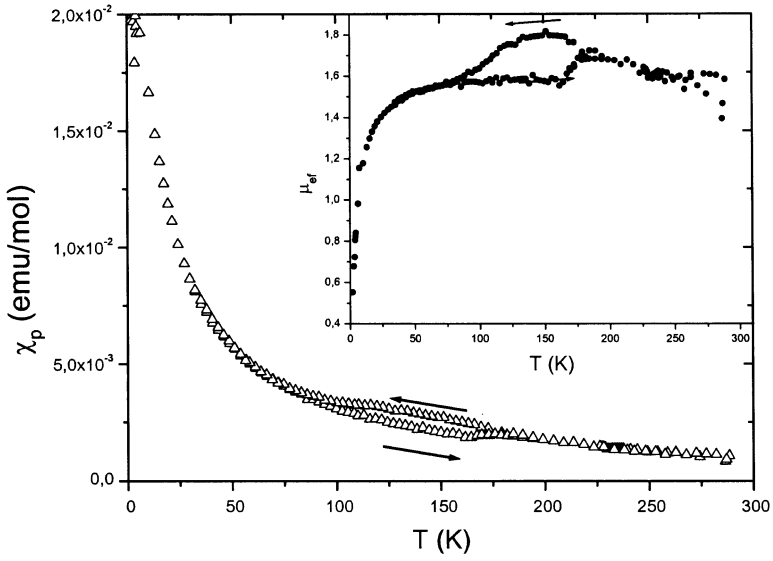

Fig. 5. Temperature dependence of the paramagnetic susceptibility, χ_p, of a polycrystalline sample of (DT-TTF)$_4$[Au(pds)$_2$]$_3$. The inset shows the effective magnetic moment.

diffraction as a function of temperature, is required to fully characterise these two transitions.

4. Supplementary material

Further crystallographic data have been deposited with the Cambridge Crystallographic Data Centre as supplementary publication no. CCDC 194 597. Copies of the data can be obtained free of charge on application to CCDC, 12 Union Road, Cambridge CB2 1EZ, UK (fax: +44 1223-336033; e-mail: deposit@ccdc.cam.ac.uk).

Acknowledgements

This work was partially supported by FCT-Portugal (Contract POCTI/35342/QUI/2000) and grants from DGI-Spain (Project BQU2000-1157), DGR Catalonia (Project 2000SGR00114). The collaboration between the team authors from Barcelona and Sacavém was supported by the ICCTI-CSIC bilateral agreement and benefited also from COST action D14.

References

[1] C. Rovira, J. Veciana, E. Ribera, J. Tarrés, E. Canadell, R. Rousseau, M. Mas, E. Molins, M. Almeida, R.T. Henriques, J. Morgado, J.-P. Schoeffel, J.-P. Pouget, Angew. Chem., Int. Ed. Engl. 36 (1997) 2323.
[2] E. Ribera, C. Rovira, J. Veciana, J. Tarrés, E. Canadell, R. Rosseau, E. Molins, M. Mas, J.-P. Schoeffel, J.-P. Pouget, J. Morgado, R.T. Henriques, M. Almeida, Chem. Eur. J. 5 (1999) 2025.
[3] G.C. Papavassiliou, S.Y. Yiannopoulos, J.S. Zambounis, Chem. Scr. 27 (1987) 265.
[4] C. Rovira, J. Veciana, E. Ribera, J. Tarrés, J. Cirujeda, E. Molins, J. Llorca, E. Espinosa, J. Org. Chem. 59 (1994) 3307.
[5] A. Altomare, M.C. Burla, M. Camalli, G. Cascarano, G. Giacovazzo, A. Guagliardi, A.G.G. Moliterni, G. Polidori, R. Spagna, J. Appl. Crystallogr. 32 (1999) 115.
[6] G.M. Sheldrick, SHELXL-97, A Program for Crystal Structure Refinement, University of Göttingen, Germany (1997).
[7] L.J. Ferrugia, J. Appl. Crystallogr. 32 (1999) 837.
[8] E. Keller, SCHAKAL-97, A Computer Program for the Representation of Molecular and Crystallographic Models, Kristallographisches Institut der Universität Freiburg i., Br., Germany (1997).
[9] E.B. Lopes, ITN Internal Report (1991).
[10] P.M. Chaikin, J.F. Kwak, Rev. Sci. Instrum. 46 (1975) 218.
[11] R.P. Huebner, Phys. Rev. 135 (1964) A1281.
[12] J.F. Kwak, G. Beni, Phys. Rev. B 13 (1976) 652.